A strain model for spall severity estimation based on FBG measurements

R. Ohana [1], R. Klein [2], J. Bortman [1], M. Tur [3]
[1] Ben-Gurion University of the Negev, Department of Mechanical Engineering,
P.O.B 653, Beer-Sheva 8410501, Israel

[2] R.K. Diagnostics,
P.O.B 101, Gilon, D.N. Misgav 20103, Israel

[3] Tel Aviv University, School of Electrical Engineering,
Ramat Aviv, 69978, Israel

Abstract
In this research, a Fiber Bragg Grating (FBG) sensor has been used for condition monitoring on spalls in deep groove ball bearings. The usage of FBG sensors is relatively new for health monitoring systems of rotating machinery. Therefore, there is not enough understanding of the strain signature measured by the FBG. To examine the phenomena in the strain signals, a physics-based model of the strain signature has been developed. In this model, two complementary models were integrated, a finite element (FE) model and a dynamic model. The strain model describes the interaction between the rolling elements (REs) and the bearing housing and simulates the strain behavior on the bearing housing. The simulation results are validated with strain signals from endurance test measured by the FBG sensor. The model allows simulation of a wide range of spall lengths. The insights from the model enabled the development of an algorithm that assesses the severity of the defect during bearing operation.

1 Introduction

Bearings are important components in rotating machinery to enable smooth operation. Failure in one of the bearings can lead to severe damage and even total failure. The most common failure mechanism in bearings is spall formation [1], where metallic particle flakes are released from the surface of the bearing raceways and/or the rolling elements (REs) [2–4]. Interactions with a defective component within a bearing lead to undesirable vibrations which increase as the defect evolves. Fault detection and diagnosis, based on vibration signals (such as, accelerometers, load cell, acoustic emission etc.), have been widely studied in the literature [5,6,15–17,7–14]. This study examines strain signals measured with Fiber Bragg Grating (FBG). FBG are small, flexible and gives a high signal to noise ratio (SNR).

Fault diagnosis of bearings via FBG sensors has not been thoroughly studied in the literature [18–20]. Numerous researchers have developed physics-based models to investigate the RE-edge impact reaction [21–24]. A fundamental study to examine the physical phenomenon in the strain signal, during the interaction of the RE with the damaged part of the bearing, is presented. In this study, a strain model has been developed and compared to the experimental strain signal measured by FBG sensors. This article deals with small spalls, such that the RE meets the spall edge before it collides with the floor of the spall.

2 Background

Strain signal has lacked interpretation in the literature. For this purpose, two complementary models were integrated into a strain model: a FE model and a dynamic model. A strain-contact force relation was developed using the FE model. This relation is multiplied by the contact force from the dynamic model to simulate the real strain behavior of the bearing house. The simulated strain and the strain signals measured by the FBG in the endurance test were compared to validate the model and to explain different phenomena detected in the strain signals. The flowchart methodology is presented in Figure 1. Based on the strain model insight, a spall size estimation algorithm was developed.

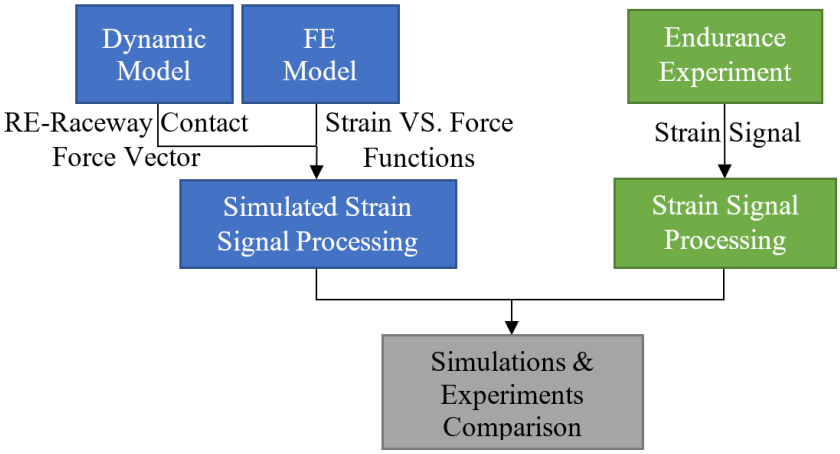

Figure 1: Research flowchart structure

2.1 FBG signal

An FBG sensor is made by the inscription of periodic variations in the index of refraction along a short section of the core of a single-mode optical fiber [25]. The strain signals measured by the FBG sensor, given by

$$\boldsymbol{\varepsilon} = \frac{\boldsymbol{\lambda_b - \lambda_0}}{\boldsymbol{C_\varepsilon \lambda_0}} \tag{1}$$

Where λ_b is the wavelength of peak reflection under strain, while λ_0 is the wavelength of peak reflection in the absence of rotation related strain. C_ε is a material constant.

2.2 Data analysis

The strain signal in the time domain was synchronized with the rotational speed signal, by angular resampling, and was transformed to the cycle domain. A de-phase algorithm [26] was applied to the strain in the cycle domain to remove the synchronous elements, e.g. shaft, that were masking the effect of the bearing in the signal. First, the synchronous average (SA) is calculated by averaging the resampled signal over a cycle of rotation. The de-phased signal is obtained by removing the SA from the angular resampled signal, leaving only the asynchronous elements. The data analysis process of the strain signal is presented in Figure 2.

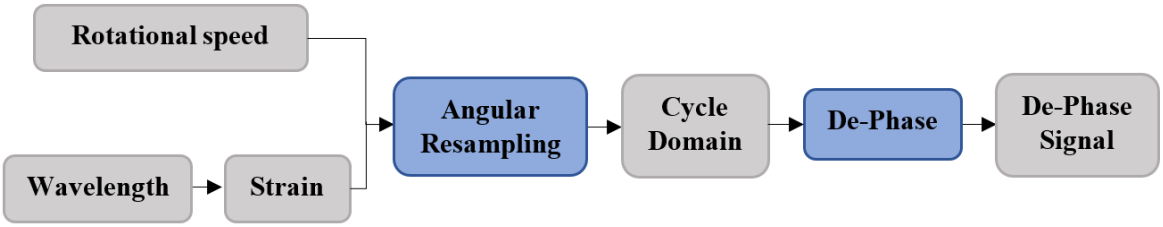

Figure 2: Strain signal analysis process

3 Endurance test

The experimental setup for the endurance test consists of a test rig and a measurement unit. The test rig includes a shaft, two support bearings, the tested bearing (6206 ETN9) and a pneumatic piston for applying different loads. All components are listed in Table 1 and marked in Figure 3. All the bearings were lubricated. A FBG sensor mounted along the bearing house of the tested bearing, see Figure 3. The sensor is connected to a Smart Fibres™ "SmartScan Aero Mini" interrogator, sampling data at 10 kS/s. To accelerate the defect initiation process, a small bore was seeded into the outer raceway of the bearing using an electrical discharge machining (EDM). The initial defect was in the center of the loading zone. The operational conditions during the test were constant with a load of 2.2 kN and the rotation speed was 35 Hz.

Figure 4 presents the strain de-phased signal at three different stages of the experiment: green signal-at the beginning of the experiment, the blue signal-at the middle of the experiment and the red signal-at the end of the experiment. All three of the signals, have a form of a periodic signal wave with BPFO frequency. An additional pulse was observed at the advanced stages of the experiment. In addition, the pulse widths and amplitude levels are higher for advanced stages of the experiment with wider spalls.

Table 1: Experimental system components

Component number	Component	Amount
1,2	Supporting bearing SYF 30 TF	2
3	Coupling	1
4	Shaft 30 mm diameter	1
5	Bearing house + tested bearing 6206 ETN9	1
6	Gear 20 teeth 2.5 module	1
7	Pneumatic piston	1
8	Three-phase motor	1

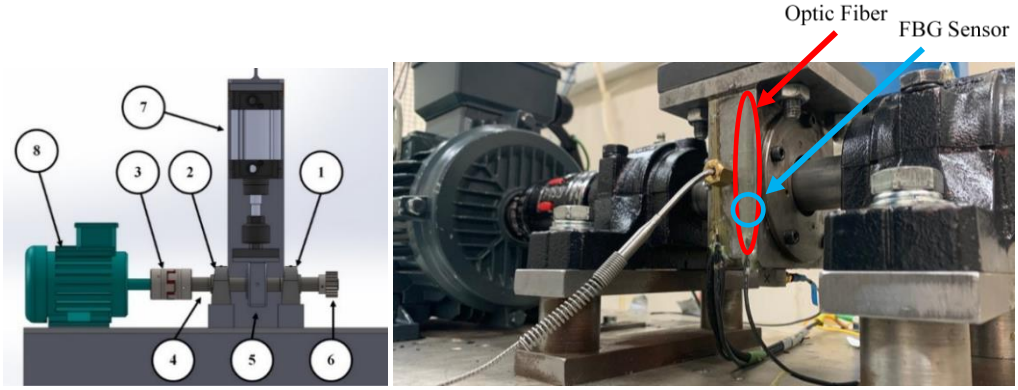

Figure 3: Endurance test rig: the component details are listed in Table 1

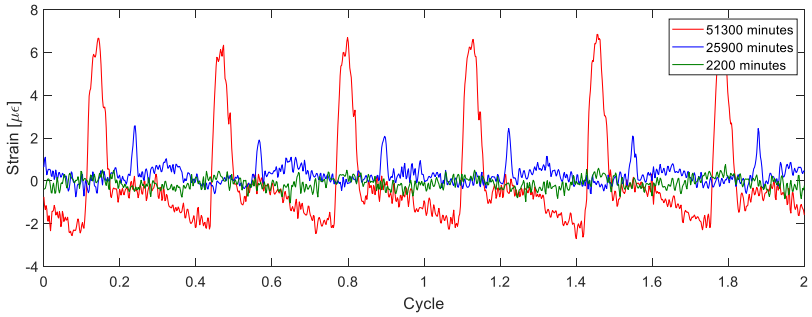

Figure 4: Strain de-phased signal at different stages during the endurance experiment

4 Strain signal model

To analyze the behavior of the measured FBG strain signals for healthy and faulty bearings, the strain model integrates between a dynamic model and a FE model as illustrated in the research flowchart diagram presented in Figure 1.

4.1 Non-linear dynamic model

A validated non-linear dynamic model was used to calculate the contact force between the RE and the outer raceway generated during the operation of both a healthy and a faulty bearing. The non-linear dynamic model developed by Kogan et al. [27], [28] is based on the classic kinematics and the dynamic equations. The boundary conditions for the dynamic model were defined according to the endurance experimental setup. Two different spall lengths were examined: 2mm and 4.8 mm. An example of the contact force of a faulty bearings with a spall length of 2mm versus the rotation angle, θ, (as illustrated in Figure 6a), of one RE is presented in Figure 6b. In Figure 6d, the green dot, and the red dot in the θ=270° region, represents the entry and exit of the RE into and from the spall, respectively. The high frequency appears in the signal is a result of the RE-spall interaction at the trailing edge. The zero force in this region represent the RE disconnection from the raceways (destressing), i.e., free flight of the RE.

4.2 FE model

A FE model was built to study the relation between (i) the contact force between the REs and the outer raceway, and (ii) the strain developed within the bearing house. The strain response location was chosen to be the same as the FBG sensor located in the test rig. A quasi-static, two-dimensional, plane strain model

was developed in ABAQUS software with the ABAQUS/standard solver. The assembly included a single RE and a bearing house (Figure 5a). The FE model geometry and dimensions presented in Figure 5a and in Table 2. The Young's modulus was taken as $E = 208\,MPa$ and the Poisson ratio was $\nu = 0.3$. An eight-node biquadratic element was used (CPE8R). A fine mesh was used in the vicinity of the contact zone and became coarser as the distance from the contact zone increased. The narrow edge was fixed at the top surface (see Figure 5a). The RE was pressed, with constant force, against the bearing house. Then, the RE was rotated 360 degrees counterclockwise with angle increments of 0.005 radians ($\Delta\theta = 0.005\,rad$) until it returned to the starting point. The simulated strain from the FE model for constant force is shown in Figure 5b. Since the contact force between the RE and the outer raceway is changing during the rotation of the RE, i.e., inside, and outside of the loading zone, the integration of the dynamic model is essential. A linear correlation between the FE strain and the constant force acting on the RE, was sought regarding the fact that, the measurement of the strain was at a far distance from the contact zone and the material is linear elastic. It is noteworthy to mention that the linear function was calculated for every angle increment.

Table 2: Model dimensions

Parameter	Comment	Value	Units
h	Bearing house height	106	mm
w	Bearing house width	100	mm
d	Bearing house depth	32	mm
D	RE diameter	11	mm
D_o	Outer race diameter	57	mm
w_1	Piston axis diameter	20	mm
N	RE number	8	-

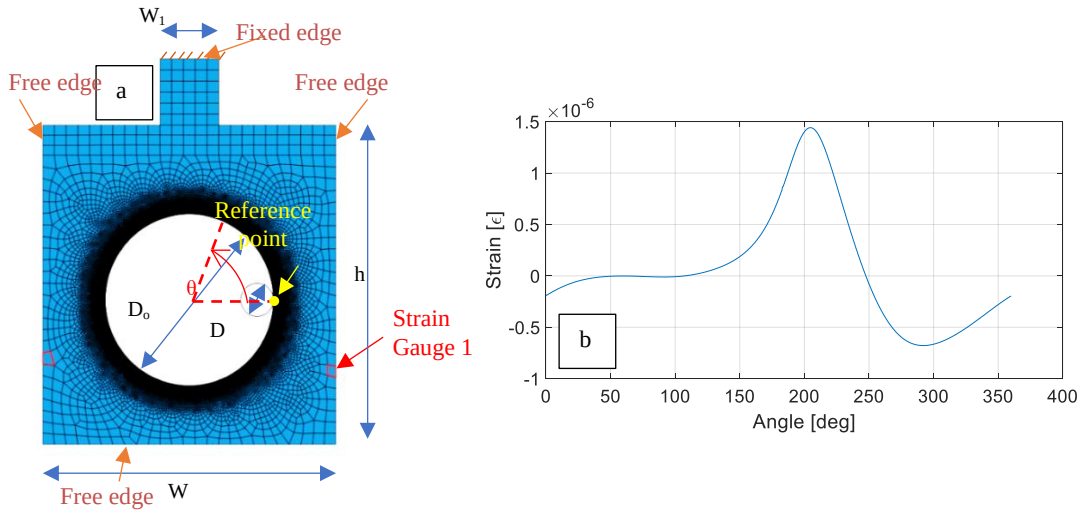

Figure 5: (a) FE model – dimensions. (b) Simulated strain results obtained from the FE model after applying a constant force of F=100 [N] on the RE

4.3 Simulated strain signal

The simulated strain signal has obtained by multiplying the contact force from the dynamic model (Section 4.1) and the slope of the linear functions from the FE model (Section 4.2) for every angle increment. An example of the simulated strain of faulty bearing with 2mm spall length is shown in Figure 6c and e. The combined effect of (i) the behavior of the contact force distribution (Figure 6b), and (ii) the behavior of the

simulated strain from the FE model (Figure 5b) is observed. The calculated strain in the faulty state (Figure 6e) has the same shape as the contact force signal in the RE-spall interaction (Figure 6d), which means that the disconnection of the RE from the raceways can also be observed in the strain signals.

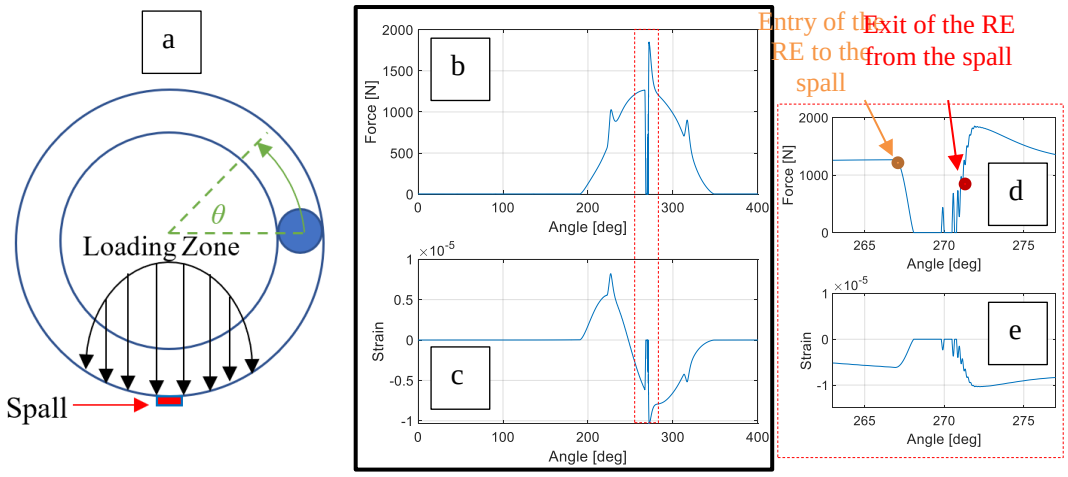

Figure 6: (a) Schematic description of the bearing (b) contact force of faulty bearing with 2mm spall length, and (c) simulated strain signal for faulty bearing, (d) and (e) close-up of the RE-spall interaction

5 Results

The model was validated by comparing the simulation results, Figure 7a, to the experiments, Figure 7b. The green curve in both graphs represent a healthy bearing and the red curve represent a faulty bearing with 4.8mm spall length. There is good agreement between the results of the simulation and the experiments, both in behavior and in scale. As illustrated in Figure 8, when a single RE reach to the spall leading edge it may impact different locations with the trailing edge. In this Figure, two examples of different impact locations are shown. For each one of the impact a different pulse width will be measured. Although the pulse width represents very well the hovering of the RE, it can give a good estimation of the spall length.

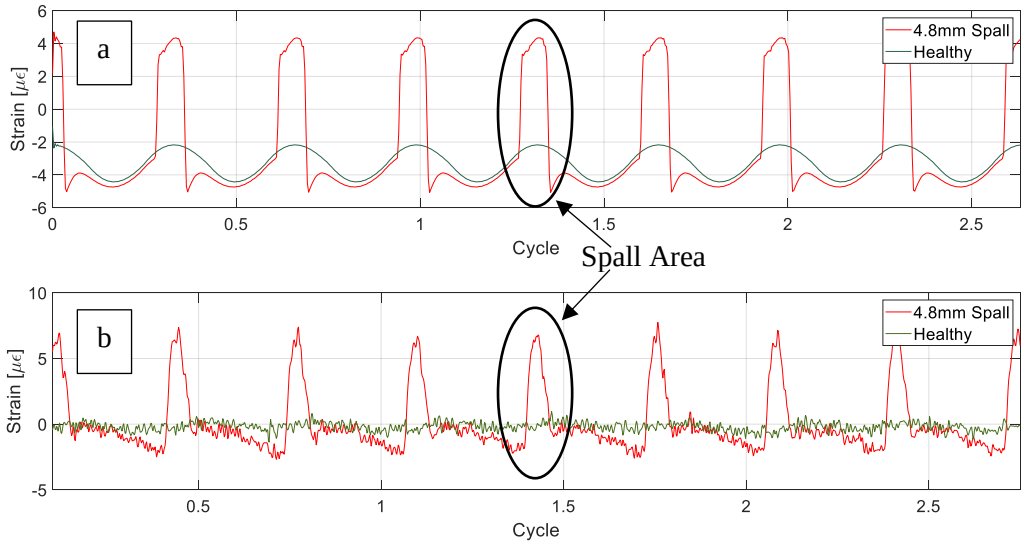

Figure 7: Comparison between: (a) simulation and (b) experimental endurance test (healthy - green and 4.8mm spall - red)

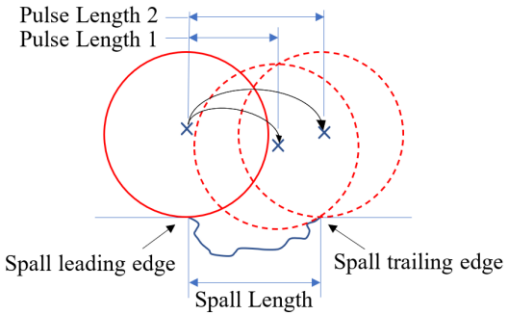

Figure 8: Illustration of a RE impact in two different possible locations at the spall edge in the experiments

6 Spall length estimation algorithm description

The spall length estimation algorithm is divided into two main stages and presented in Figure 9: (i) selection of the RE-spall interactions and (ii) evaluation of the pulse width that represents the RE flight. The selection of the RE-spall interactions is performed on the squared de-phased strain signal, x^2, in order to emphasize the pulses in the strain signal. Since the spall is located on the outer raceway of the bearing, it is possible to detect BPFO interactions in one cycle. A dynamic threshold, which is a percentage of the highest value in the signal, is used to determine which peaks represent the correct interactions. After the RE-spall interaction has been detected, the algorithm searches the entrance and the exit points of the RE into the spall by defining the first negative minimum adjacent to the peak of the pulse. The evaluated pulse width, that it is assumed to be the spall length, is obtained by the average of all the estimated pulse widths.

The pulses started to be observed in the signals after 24,000 minutes, therefore, the algorithm was applied to all the strain de-phased signals after 24,000 minutes. Figure 10 presents the algorithm output which is a trend line of the estimated spall length. The trend line is approximately monotonic as expected. The minimal spall length that could be estimated by the algorithm was 1.6 mm. After the bearing was disassembled, a 5.1 mm spall was measured, while the estimated fault length was 5.4 mm. The approximation error is close to 6%.

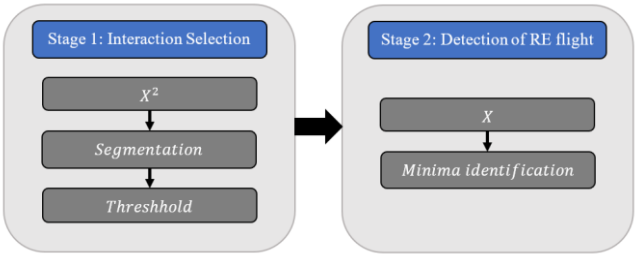

Figure 9: Algorithm stages for spall length estimation in the bearing outer race for the strain signal

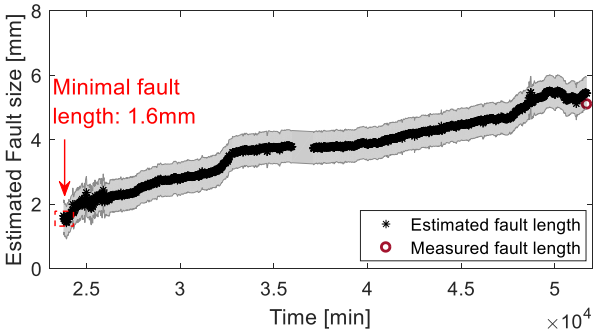

Figure 10: Trend line of the fault length estimation during the endurance experiment

7 Summary and concussions

This study examines the strain signals of healthy and faulty bearings, for diagnostic capabilities via FBG sensors. The theoretical analysis is based on two complementary models that were integrated into a strain model. The validation of the model has been done by comparing the simulation results with the endurance test results. Based on the model insights, it was possible to determine that the additional pulses correspond to the free flight of the ball over the spalled area. In addition, the pulse width is directly related to the arc length of the free flight of the ball. Based on the strain model, a reliable algorithm for spall length estimation has been developed.

Acknowledgements

I gratefully express my deepest appreciation to the Pearlstone Center for their support and funding of this work.

References

[1] B. Jalalahmadi, F. Sadeghi, T. S. Slack, N. Raje, and N. K. Arakere, "A Review of Rolling Contact Fatigue," *Artic. J. Tribol.*, 2009.

[2] N. Raje, T. Slack, and F. Sadeghi, "A discrete damage mechanics model for high cycle fatigue in polycrystalline materials subject to rolling contact," *Int. J. Fatigue*, vol. 31, no. 2, pp. 346–360, Feb. 2009.

[3] D. Gazizulin, R. Klein, and J. Bortman, "Towards efficient spall generation simulation in rolling element bearing," *Fatigue Fract. Eng. Mater. Struct.*, vol. 40, no. 9, pp. 1389–1405, 2017.

[4] L. Rosado, N. H. Forster, K. L. Thompson, and J. W. Cooke, "Rolling contact fatigue life and spall propagation of AISI M50, M50NiL, and AISI 52100, part I: Experimental results," *Tribol. Trans.*, vol. 53, no. 1, pp. 29–41, 2010.

[5] H. Zhang *et al.*, "A benchmark of measurement approaches to track the natural evolution of spall severity in rolling element bearings," *MSSP*, vol. 166, p. 108466, Mar. 2022.

[6] H. Zhang, P. Borghesani, W. A. Smith, R. B. Randall, M. R. Shahriar, and Z. Peng, "Tracking the natural evolution of bearing spall size using cyclic natural frequency perturbations in vibration signals," *Mech. Syst. Signal Process.*, vol. 151, Apr. 2021.

[7] L. Cui, Y. Zhang, F. Zhang, J. Zhang, and S. Lee, "Vibration response mechanism of faulty outer race rolling element bearings for quantitative analysis," *J. Sound Vib.*, pp. 1–10, 2015.

[8] R. B. Randall, "Vibration-based Condition Monitoring : Industrial, Automotive and Aerospace Applications.," p. 309, 2011.

[9] R. B. Randall and J. Rôme Antoni, "Rolling element bearing diagnostics-A tutorial," 2010.

[10] W. Wang, N. Sawalhi, and A. Becker, "Size Estimation for Naturally Occurring Bearing Faults Using Synchronous Averaging of Vibration Signals," *J. Vib. Acoust. Trans. ASME*, vol. 138, no. 5, Oct. 2016.

[11] B. Eftekharnejad, M. R. Carrasco, B. Charnley, and D. Mba, "The application of spectral kurtosis on Acoustic Emission and vibrations from a defective bearing," *Mech. Syst. Signal Process.*, vol. 25, pp. 266–284, 2010.

[12] C. Qing, S. Eryn, Z. Dongmei, G. Juwen, and F. Zhonghe, "Measurement of the critical size of inclusions initiating contact fatigue cracks and its application in bearing steel," *Wear*, vol. 147, pp. 285–294, 1991.

[13] C. Tarawneh, J. D. Lima, N. D. L. Santos, and R. E. Jones, "Prognostics Models for Railroad Tapered Roller Bearings with Spall Defects on Inner or Outer Rings," *Tribol. Trans.*, vol. 62, no. 5, pp. 897–906, 2019.

[14] M. L. French and W. M. Hannon, "Angular contact ball bearing experimental spall propagation observations," *J. Eng. Tribol.*, vol. 229, no. 8, pp. 902–916, 2015.

[15] L. Zhen, H. Zhengjia, Z. Yanyang, and C. Xuefeng, "Bearing condition monitoring based on shock pulse method and improved redundant lifting scheme," *Math. Comput. Simul.*, vol. 79, pp. 318–338, 2008.

[16] I. El-Thalji and E. Jantunen, "Fault analysis of the wear fault development in rolling bearings," 2015.

[17] R. B. R. W.S. Siew, W.A. Smith, Z. Peng, "Fault severity trending in rolling element bearings - University of New South Wales," 2015.

[18] H. Alian, S. Konforty, U. Ben-Simon, R. Klein, M. Tur, and J. Bortman, "Bearing fault detection and fault size estimation using fiber-optic sensors," *Mech. Syst. Signal Process.*, vol. 120, pp. 392–407, Apr. 2019.

[19] P. Wei, Z. Dai, L. Zheng, and M. Li, "Fault diagnosis of the rolling bearing with optical fiber Bragg grating vibration sensor," in *Optical Measurement Technology and Instrumentation*, Oct. 2016, vol. 10155, p. 101552I.

[20] M. Khmelnitsky, J. Bortman, U. Ben-Simon, R. Klein, and M. Tur, "Improved bearing sensing for prognostics: From vibrations to optical fibres," in *Insight: Non-Destructive Testing and Condition Monitoring*, Aug. 2015, vol. 57, no. 8, pp. 437–441.

[21] N. Branch, N. K. Arakere, V. Svendsen, and N. H. Forster, "Stress field evolution in a ball bearing raceway fatigue spall," *J. ASTM Int.*, vol. 7, pp. 1–18, 2009.

[22] N. K. Arakere, N. Branch, G. Levesque, V. Svendsen, and N. H. Forster, "Rolling contact fatigue life and spall propagation of AISI M50, M50NiL, and AISI 52100, part II: Stress modeling," *Tribol. Trans.*, vol. 53, no. 1, pp. 42–51, 2009.

[23] N. A. Branch, N. K. Arakere, N. Forster, and V. Svendsen, "Critical stresses and strains at the spall edge of a case hardened bearing due to ball impact," *Int. J. Fatigue*, vol. 47, pp. 268–278, 2013.

[24] D. Gazizulin, L. Rosado, R. Schneck, R. Klein, and J. Bortman, "A new efficient rolling element – Spall edge interaction model," *Int. J. Fatigue*, vol. 131, p. 105330, Feb. 2020.

[25] K. O. Hill and G. Meltz, "Fiber Bragg grating technology fundamentals and overview," *J. Light. Technol.*, vol. 15, no. 8, pp. 1263–1276, Aug. 1997.

[26] R. Klein, E. Rudyk, E. Masad, and M. Issacharoff, "Emphasising bearing tones for prognostics," *Int. J. Cond. Monit.*, vol. 1, no. 2, pp. 73–78, Nov. 2011.

[27] G. Kogan, R. Klein, A. Kushnirsky, and J. Bortman, "Toward a 3D dynamic model of a faulty duplex ball bearing," *Mech. Syst. Signal Process.*, vol. 54, pp. 243–258, Mar. 2015.

[28] G. Kogan, J. Bortman, and R. Klein, "A new model for spall-rolling-element interaction," *Nonlinear Dyn.*, vol. 87, no. 1, pp. 219–236, Jan. 2017.